HHS Public Access

Mnemonic representations of transient stimuli and temporal sequences in the rodent hippocampus *in vitro*

Robert A. Hyde and **Ben W. Strowbridge**

Department of Neurosciences Case Western Reserve University Cleveland, OH, USA

Abstract

A primary function of the brain is to store and retrieve information. Except for working memory, where extracellular recordings demonstrate persistent discharges during delay-response tasks, it has been difficult to link memories with changes in individual neurons or specific synaptic connections. Here, we demonstrate that transient stimuli are reliably encoded in the ongoing activity of brain tissue *in vitro*. We found that the patterns of synaptic input onto dentate hilar neurons predict which of four pathways were stimulated with an accuracy of 76% and performed significantly better than chance for >15 s. Dentate gyrus neurons also could accurately encode temporal sequences using population representations that were robust to variation in sequence interval. These results demonstrate direct neural encoding of temporal sequences in the spontaneous activity of brain tissue and suggest a novel local circuit mechanism that may contribute to diverse forms of short-term memory.

A fundamental property of the central nervous system is the ability to encode and retrieve information. In mammals, declarative memory function is typically divided into behavioral tasks that promote short- or long-term storage of items such as names, places and specific temporal sequences[1,2]. While the specific cellular origin of individual long-term declarative memories has remained elusive, a large literature highlights the importance of several critical brain regions, including the prefrontal cortex [3] and the hippocampal formation[4] for encoding short-term, or working, memories. Extracellular unit recordings in these brain areas often display periods of persistent spiking activity at elevated frequencies when animals are required to retain transiently presented sensory information. This "delay-period activity" typically lasts for seconds and is extinguished when the animal initiates a behavioral response to indicate whether it correctly remembered the correct transient stimulus[3,5]. The reduction in persistent spiking during error trials—trials in which the animal made an incorrect behavioral response following the delay period—argues that delay-period activity in those specific neurons reflects activity in neural circuits encoding that short-term memory, rather than a response to the cue stimulus or a motor plan

Correspondence: Dr. Ben W. Strowbridge Dept. of Neurosciences Case Western Reserve University 10900 Euclid Ave. Cleveland, OH 44106 USA bens@case.edu Phone: 216-368-6974 .

associated with the behavioral output. These classic studies in primates, along with more recent reports in rodents[6–8], remain one of the clearest examples in which the spiking activity of individual neurons can be directly tied to specific memories.

While abundant evidence relates delay-period persistent spiking activity to short-term memories, the underlying cellular mechanisms that mediate this firing mode have not been determined. Donald Hebb postulated in 1949[9] that short-term memories could be maintained by reverberant activity that circulates through networks of interconnected excitatory neurons. Indeed, transient stimuli can trigger persistent spiking activity in artificial neural networks that contain recurrent excitatory connections[10–13] although maintaining stable firing frequencies in individual circuit elements during the storage operation requires highly precise tuning of synaptic connection strengths[10,14,15]. Some types of CNS neurons also contain constellations of intrinsic conductance that enable them to maintain simple memories by firing persistently for several seconds following transient depolarizing stimuli even when pharmacologically isolated from all other neurons[16,17]. Computational models that combine individual simulated neurons with intrinsic persistence and recurrent excitatory connections are capable of generating persistent firing modes without the high connection weight tuning precision required to enable simple associative network models to fire persistently[11,14,18,19]. While biological experiments have demonstrated examples of both intrinsic persistence[16,17,20] and recurrent excitatory connections[21–23] in different brain regions, the absence of a tractable *in vitro* system capable of short-term information storage has limited the opportunities to determine which specific mechanisms are required to generate short-term mnemonic representations of transient stimuli.

Here, we demonstrate that four distinct patterns can be reliably encoded within the spontaneous synaptic activity in conventional rodent hippocampal slice preparations. Each pattern is evoked by briefly activating a different subset of entorhinal input axons (the perforant path, PP) using an array stimulation electrode; information is read out by recording intracellularly from two or three dentate hilar neurons, which sample the activity of both dentate granule cells[24] and semilunar granule cells (SGCs; Fig. 1a), a recently-discovered excitatory cell type that responds to PP stimulation with graded depolarizing plateau potentials[20,25,26]. We find that synaptic barrages evoked in downstream hilar neurons by persistent firing in SGCs reliably encode both the identity of individual stimuli and temporal sequences of PP stimuli. Decoding both individual stimuli and temporal sequences relied on population representations of synaptic inputs to dentate hilar cells. Short-term encoding of sequences was robust to perturbation of sequence interval, suggesting that contextual coding in these experiments arises from stimulus order rather than the delay between stimuli. While several *in vivo* recording studies suggested that neurons in the hippocampal formation are involved in short-term memory function[4,7], these results provide the first demonstration that neural networks within the dentate gyrus are capable of encoding both multiple transient inputs and context-dependent information such as the order of temporal sequences.

RESULTS

The dentate gyrus supports multiple distinct neural representations

Transient stimulation of the perforant path (2×200 μs shocks) leads to sustained increases in the frequency of spontaneous EPSPs recorded in dentate hilar neurons over multiple seconds (Fig. 1b), as described in a recent report[20]. That study found that the circuitry contained in a conventional hippocampal slice preparation could encode two distinct activity patterns. Here, we first asked whether more than two patterns could be encoded in the dentate gyrus and what factors govern coding accuracy.

Hilar cell responses to stimuli at different PP locations were recorded after placing an array electrode (4 contacts, 115 μm spacing) in the middle molecular layer of the dentate gyrus. Activation of each electrode contact (A, B, C, or D) individually typically elicited synaptic barrages (average EPSP frequency of spontaneous EPSPs in barrage = 18.7±0.5 Hz vs. 3.0±0.1 Hz immediately before PP stimulation; $P<0.0001$; n=33 cells). The 3.5 min interval between episodes was significantly longer than synaptic barrages triggered by PP stimuli (decay tau ~8 s,[20]) and we did not observe steady changes in baseline EPSP frequency during experiments. While responses evoked by different electrodes in this experiment had different mean EPSP frequencies, the range of EPSP frequencies in each response overlapped (Fig. 1c-d) and were only infrequently statistically separable (see below).

We next asked if the separation of responses evoked by stimuli at different locations could be increased by sampling the hilar network more densely using multiple simultaneous intracellular recordings (Fig. 2a, Supplemental Fig. 1). Using this approach, responses to each stimulus in an experiment could be plotted in the 3-dimensional space formed by the frequency of EPSPs recorded in each of three hilar neurons during the initial 4 s after the stimulus (Fig. 2b). In most experiments, including the example shown in Fig. 2b, responses to each stimulus type were clustered in different regions within the 3-dimensional plot of EPSP frequency in each hilar cell. By analyzing synaptic responses of hilar networks in EPSP frequency space, we can directly apply standard statistical and clustering methods along biologically-meaningful dimensions without requiring dimensionality reduction techniques such as principal component analysis. Since the presentation order was randomized, response clustering was unlikely to represent short-term plasticity associated with repeated stimulation at the same location.

While many experiments yielded visually distinct response clusters from each stimulus location, as in Fig. 2b, linear discriminant analysis (LDA) offers a rigorous method to determine whether specific pairs of responses to different stimulus locations (A/B, B/C, etc) were statistically separable. Statistical significance on 6 pairwise LDA tests are required to completely separate the responses to all four stimuli ($P<0.0083$ for each LDA test, reflecting a Bonferroni correction for multiple comparisons). This criterion was met in 50% of the experiments analyzed (6/12; EPSP frequencies assayed in initial 4 s of each response; Fig. 2c), indicating that the ability of the dentate gyrus to generate short-term representations of 4 transient inputs is robust. Responses to three stimuli were statistically separable in half of the remaining 6 experiments (3/12 experiments). On average, we obtained 4.8±0.5 out of the 6 separation planes required to separate four response patterns, compared with 0.83 planes

expected by chance ($P<0.001$; $n=12$ experiments, 9 triple recordings and 3 paired recordings; see Online Methods for details). Our ability to statistically separate four patterns was greatest (5.6±0.7 significant planes) when we only considered the 9 experiments with simultaneous triple recordings. Eliminating data from one or two neurons in the 9 triple recording experiments substantially degraded the statistically separate responses to different stimuli (Fig. 2d); synaptic barrages recorded from one hilar neuron typically were only able to discriminate between two out of the four response patterns (1.7±1.4 statistically significant planes; Fig. 2d).

The ability of hilar networks to create mnemonic representations of transient stimuli was relatively independent of the window duration over which EPSP frequency was analyzed (Supplemental Fig. 2), with only a minor (13.8 %) reduction in the number of significant LDA planes obtained with 1 s analysis windows, compared with 4 s windows used in the initial analysis. We next conducted a separate set of triple recordings at relatively depolarized membrane potentials (~-60 mV) using two stimulus locations to ask if stimulus identity also was represented in the spike output of hilar cells. In each experiment in which responses to *A* and *B* stimuli were separable using LDA of EPSP frequency across the three cells ($n=3$; LDA p values ranged between 2.0×10^{-9} and 2.2×10^{-4}), we found stimulus-specific suprathreshold responses based on spike frequency assayed in the same 4 s window (LDA p values ranged between 0.002 and 0.016; mean spike frequency 3.0 Hz following PP stimuli versus 0.06 Hz in control conditions). These results demonstrate that both the synaptic input to hilar cells and the resulting spike output can represent stimulus identity. We also found significantly more variation between responses from different stimulus locations than responses evoked by the same location using an omnibus measure of response separation (OVL, 12/12 experiments with p(OVL)<0.05; Fig. 2e and see Supplemental Fig. 3) that is used to assay overlapping distributions. Responses to the four stimuli were not separable based on LDA of baseline (pre-stimulus) EPSP frequencies (mean 1.0 plane; significantly different from the number of planes from stimulus responses; $P<0.0001$). The stimulus intensities used to evoke synaptic barrages were not significantly different on each contact (F=1.23; $P>0.05$; one-way ANOVA; $n=180$). These results demonstrate that transient stimuli activating 4 different sets of entorhinal inputs to the dentate gyrus resulted in at least 3 distinct patterns of hilar synaptic activity in a majority of experiments; all four responses were statistically separated in 50% of the experiments (Fig. 2c).

We next assayed the accuracy of recall based on comparing individual responses to the average response recorded at each stimulus location. We first tested the accuracy of response classification by predicting stimulus identity based on the nearest average response (centroid) computed from the first 4 s of each response (Fig. 3a). In this decoding method, if a response triggered by an *A* stimulus was closest to the average response to all *A* stimuli, the analysis would generate a correct *A* prediction. By contrast, if the response triggered by that stimulus was closest to the average response of all *C* trials in that experiment, then an incorrect prediction (that the response was triggered by *C* instead of the correct answer, *A*) would be recorded. Over all 12 experiments, this method predicted which one of the 4 possible stimulus locations was activated with an accuracy of 76.1% ($n=180$ trials with 137 correct and 43 incorrect predictions). This prediction accuracy is significantly greater than

the 25% accuracy expected by chance (S.D. = 3.2%; $P<0.0001$; also significantly greater than the accuracy obtained following shuffling stimulus identities; $P<0.0001$; Fig. 3b). We did not observe a correlation between the physical distance between pairs of stimulating electrodes tested and the Euclidean distance between the resulting synaptic barrages (Fig. 3c). Neither was there a correlation between the inter-electrode distance and the accuracy differentiating hilar responses (e.g., *A/B* was differentiated as accurately as *A/D*; Fig. 3d). These results demonstrate that the dentate gyrus can generate distinct and repeatable population responses patterns even when nearby stimulation electrodes are activated, arguing that separation of network states in EPSP frequency space is not related to the physical separation between the stimulating electrodes used.

Origin of recall errors

We next focused on the 43 trials with classification errors to determine the factors that govern accuracy of short-term information storage in the dentate gyrus. In Fig. 3e, we plotted the distance between response pairs that were always correctly classified (black symbols) and those that were misidentified at least once in an experiment (red symbols). While the range of mean Euclidean distances between responses that were accurately predicted spanned 50 Hz, all classification errors arose from experiments where average responses between pairs of stimuli were separated by less than 30 Hz. The distance between average responses that were misidentified (10.2 ± 1.0 Hz; *n*=43) was significantly less than the distance between responses that were always correctly classified (21.6 ± 1.3 Hz; *n*=44; $P<0.002$). Half of all errors occurred when discriminating between two average responses separated by less than 7 Hz (Fig. 3f).

These results suggest that one factor governing mnemonic coding accuracy is the separation of responses to different stimuli in EPSP frequency space. While restricting recall tests to trials with well-separated average responses improved accuracy (not shown), there was a relatively poor correlation between the distance between pairs of average responses and the accuracy differentiating between those responses ($R^2 = 0.13$; $P>0.05$; Fig. 3g). This model of variation in accuracy also did not predict the average separation between centroid pairs that were always classified correctly (black symbol). However, scaling the distance between responses by the pooled variance of each response improved the correlation with accuracy ($P<0.0001$; F=33.1; Fig. 3h). Moreover, this model, based solely on imperfectly classified trials, predicted the scaled distance between perfectly classified trials (black symbol). These results suggest that much of the variability in recall accuracy (62% of the variance) can be explained by a simple two-component model based on the Euclidean distance between average responses and the scatter around those average responses.

Time course of response separability

Synaptic barrages evoked by PP stimuli decayed with an average tau of ~ 8 s[20] and decreased to 39.8% of the initial frequency after 18 s in the present study (*n*=12 cells; Fig. 4a). When displayed in 3-dimensional EPSP frequency space (Fig. 4b), average responses evoked by different stimulating electrodes followed distinct trajectories toward the origin and did not coalesce even though overall EPSP frequency decreased continuously in all responses. We next asked how long hilar responses evoked by different electrodes remain

statistically separable and found that hilar networks could still represent information > 4 s after transient molecular layer stimulation, despite decreasing synaptic drive. The mean number of separable responses decreased from 3.25 to 2.25 over 18 s (black symbols in Fig. 4c). Three experiments maintained perfect response separation (4 separable responses, 6/6 significant planes; red plot in Fig. 4c) for 8 s. Overall classification accuracy decreased to 55.3% at 18 s after stimulation (*n*=12 experiments). The duration representations remained distinct was inversely correlated with initial pattern overlap (Fig. 4e; $R^2 = 0.62$; F=15.4; *P*<0.005), suggesting that hilar networks reliably encode over time stimuli that create highly disparate responses. We also tested whether responses to different stimuli could be differentiated across different time windows (e.g., *A* at 5 s versus *B* at 8 s). The analysis presented in Supplemental Fig. 4 suggests that responses to different stimuli remain distinct across different times (no statistically significant difference between same-time and different time pairwise comparisons; *P*>0.7; K-S test).

The ability of the rodent dentate gyrus to encode four representations following transient molecular layer stimulation is shown graphically in Supplemental Fig. 5. Each possible stimulus location is represented by a character (A-D) whose contrast is a function of the distance to the average response (see Online Methods). A trial with a population response very close to the mean response to stimulus *B* would be represented by a dark "B" superimposed on dim "A", "C", and "D" characters. This method illustrates both the high accuracy of dentate representations of stimulus identity (only 1 of 14 consecutive trials was incorrect) and the persistence of the population coding in the dentate hilus. This visual analysis was cross-validated in in Fig. 5, where half the data set was used to compute mean response centroids and the other half used to generate the character display.

Dentate gyrus circuits encode temporal sequence order

Besides representing individual stimulus positions, hilar networks reliably encoded different temporal sequences. Distinct hilar up-states were evoked by activation of the same four stimuli in different order (*ABCD* vs. *DCBA*; Fig. 6a-b). Hilar synaptic responses to forward- and reverse-order sequences were clustered and reproducible (Fig. 6c; 5 s intervals) and could be statistically separated using the same LDA methods used to analyze responses to individual stimuli. Responses to forward- and reverse-order sequences were statistically separable in 10 of 11 hilar triple recording experiments (at least *P*<0.05; Fig. 6d). Sequence separability did not reflect simply the differences between the final responses in each sequence. In 8 of the 11 experiments, the sequence response was statistically different from the response to the final stimulus presented in isolation. Sequence identity was accurately predicted on the basis of hilar synaptic responses (classification accuracy = 95.6±1.9 %; significantly greater than expected by chance; *P*<0.0001; *n*=11 experiments). Synaptic barrages associated with sequential stimulation were blocked by the NMDA receptor antagonist MK801 (10 μM; Fig. 6e), as described previously for responses to single location stimuli [20]. Blockade of NMDA receptors did not affect the basal frequency of AMPA receptor-mediated EPSPs recorded in hilar neurons (P > 0.05; Fig. 6e pre-sequence bars), suggesting that this treatment suppressed stimulus-evoked network up-states.

Hilar representations of temporal sequences did not arise from simple summation of invariant responses to individual stimuli. Rather, responses to each stimulus varied greatly depending on the temporal order within the sequence (Fig. 6f), suggesting that responses to specific stimuli reflected sequence history. While the magnitude of the change in the hilar response tended to decline with each successive stimulus in the train (20.2% mean reduction during each interval), the average magnitude change following the fourth stimulus was still significantly above the basal frequency of spontaneous EPSPs (3.3±0.5 Hz; *P*<0.0001; *n*=11 experiments). The history dependence of responses to stimulus sequences was evident when vector representations of responses were added head-to-tail (Fig. 6g) and also when responses to the same stimuli were plotted from the same origin (Supplemental Fig. 6). Over 11 triple recording experiments, hilar sequence responses significantly diverged following the second stimuli (Fig. 6h) and failed to converge at the end of the sequence. (Convergence would be expected if responses to sequential stimuli were commutative.) Increasing the inter-stimulus interval from 5 to 120 s eliminated most of the history dependence (Fig. 6g-h), suggesting a temporal limit to the ability of the dentate gyrus to encode sequential stimuli *in vitro*. We also found statistically-significant sequence-specific hilar responses when forward and reverse sequential stimuli were repeated at 8 s intervals (3 of out 3 experiments with LDA p values < 0.05; Supplemental Fig. 7) but only infrequently using 2 s intervals (1 of 3 experiments with *P*<0.05; Supplemental Fig. 8).

Sequence classification accuracy (forward or reverse) also was robust to small perturbations of inter-stimulus interval. Intracellular responses of hilar cells to shortened *DCBA* stimulus trains (4 s instead of the standard 5 s interval) more closely resembled responses to standard *DCBA* than to *ABCD* stimulus trains (Fig. 7a). Population responses to shortened (4 s) *DCBA* trains also overlapped with responses to 5 s *DCBA* stimuli in EPSP frequency space (Fig. 7b) and were closer to the centroid of the 5 s *DCBA* response than to the 5s *ABCD* response (Fig. 7c). In 5 experiments tested, the plane generated by LDA of sequences with 5 s inter-stimulus intervals accurately classified 4 s reverse sequences (85.4±9.0 % correct; purple bar in Fig. 7d; not significantly different than the overall accuracies classifying 5-s interval stimulus trains; green and orange bars in Fig. 7d; *P*>0.05). These results demonstrate that synaptic responses recorded in small groups of hilar neurons *in vitro* can encode both stimulus and sequence identities and are robust to variations in sequence interval.

Population representations of biological information in the dentate gyrus

Hilar representations of stimulus information could arise from a simple coding strategy based on the magnitude of the distinct EPSP frequencies across hilar cells. Alternatively, stimulus location and sequence information could be encoded by diverse population activity patterns reflecting differential responses in individual hilar neurons (Fig. 8a). We first asked if eliminating the information associated with differences in vector magnitude impaired information encoding. Responses to each of 4 stimulus locations remained well clustered following vector normalization (two examples shown in Fig. 8b). The wide distribution of vector directions over 9 triple recording experiments (Fig. 8c) suggests there was minimal systematic bias to generate clusters in one particular region. Eliminating response magnitude information only slightly reduced the number of significant LDA separation planes (from

4.8±0.5 to 3.9±0.7; *P*>0.05; *n*=12; Mann-Whitney; Fig. 8d) while eliminating vector direction information (retaining only vector magnitudes) significantly impaired response discrimination (1.4±0.4 planes; significantly less than both actual and normalized; *P*<0.01). Normalized population responses also tracked actual discrimination performance well over time (Fig. 8e) and remained significantly above chance performance over the time period analyzed. Hilar responses to sequential stimuli were similarly robust to normalization (10/11 experiments with separable forward and reverse responses following magnitude normalization; *P*<0.05 from LDA), implying that the dentate gyrus uses primarily distributed population codes to represent stimulus information in these experiments. Sequence identity was classified accurately in both control and normalized conditions over 6 s and prediction accuracy remained significantly better than expected by chance over the time window tested (Fig. 8f).

DISCUSSION

We find that dentate hilar neurons reliably encode information as distinct patterns of spontaneous synaptic activity that persist for seconds and that resemble the persistent activity patterns recorded in nonhuman primates[3,4,27] and rodents[7] during cross-modality working memory tasks. The same cellular mechanism that encodes isolated stimuli appears also to generate reliable contextual representations of stimuli presented within temporal sequences. Responses of dentate hilar neurons accurately predicted the identity of sequences of stimuli, were distinct from responses to the final stimulus presented in isolation in most experiments, and were robust to perturbation of sequence interval. Our results suggest that both sequential and non-sequential information were represented by population codes in the dentate gyrus.

Information representation in the dentate gyrus in vitro

While hilar synaptic barrages have been reported previously in response to PP stimulation[20], this study is the first to demonstrate that changes in the ongoing synaptic input to dentate gyrus neurons can encode both the identity of more than two stimuli presented individually and in temporal sequences. Stimulus-evoked synaptic barrages reliably represented information that could be decoded using a standard classification method[28] assaying the Euclidean distances between a response in a single trial and the four centroids that reflect average responses to the four stimuli. The classification accuracy we found using this unbiased decoding approach (~76% correct trials) was significantly greater than expected by chance; high classification accuracy was maintained when we constructed a naïve decoder based on centroids computed from half of the data set (Fig. 5). The success of this simple, distance-based decoder was unexpected given the small number of nearby hilar cells sampled and argues that the ability of the dentate gyrus to generate multiple distinct activity patterns is robust and is preserved in acute hippocampal slice preparations. While experimental limitations restricted these experiments to assaying closely-spaced groups of neurons, asking whether widely-separated populations of hilar cells also can represent information should be possible in future experiments using optical activity probes. The success of the decoding method employed in this study suggests that the separation between different population response patterns is typically large enough to overcome noise and any

potential synaptic plasticity associated with repeated trials in the same experiment. Most decoding errors occurred in experiments where pairs of response centroids occupied similar locations within EPSP frequency space (Fig. 3e-f). A simple model that included both the separation between centroids and the dispersion of individual responses around each centroid[28] predicted the minimal inter-centroid distance required for reliable (error-free) decoding (Fig. 3h).

In addition to assessing accuracy using a Euclidean distance-based decoder, we used two independent methods (overlap coefficient, OVL and linear discriminant analysis, LDA) to test whether hilar population responses evoked by different stimuli were distinct. These methods demonstrated that responses evoked by individual stimuli or temporal sequences of stimuli were statistically separable in most experiments. Our experiments took advantage of intracellular recordings to reveal the underlying synaptic events that excite hilar neurons, rather than inferring synaptic drive from extracellularly-recorded spiking activity. One tradeoff with this approach, however, is the limited time over which three simultaneous intracellular recordings could be maintained (typically 60-90 min). This limitation restricted our ability to gather the hundreds of repetitions typically required for rigorous information-theoretic analysis.

Previous work demonstrated that PP-evoked synaptic barrages are unlikely to result from recurrent excitatory connections. The majority of mossy cell axonal projections are to contralateral and distal ipsilateral granule cells[29]—projections that are largely absent in the transverse hippocampal slices employed in this study. The local projections of glutamateric hilar mossy cells are primarily to GABAergic interneurons and only infrequently (0.5% connection probability) form recurrent monosynaptic connections onto other nearby mossy cells[30]. Instead, hilar synaptic barrages appear to result from persistent spiking activity in semilunar granule cells (SGCs), a newly-discovered excitatory cell type in dentate molecular layer[25,26]. SGCs in the molecular layer respond to transient PP stimuli with depolarizing plateau potentials that require L- and T-type voltage-gated calcium channels[20]. Granule cells, by contrast, are typically inhibited by PP stimuli that trigger hilar synaptic barrages. Both granule cells and SGCs are polarized neurons whose axonal arbors are excluded from regions containing their own somatodendritic compartments[25,26], indicating that neither cell type forms recurrent excitatory connections. Our ability to trigger statistically separable hilar population responses may result from recruitment of persistent spiking activity in different subsets of SGCs that project diffusely to hilar neurons. Alternatively, the distinct patterns we observe may result from stimulus-specific graded plateau depolarizations[20] within a uniform subset of SGCs or from differential activation of inhibitory local circuits. Further experiments monitoring larger subsets of dentate gyrus neurons will be required to determine the extent of the SGC network excited by different stimuli in order to distinguish among these hypotheses.

Previous *in vitro* work in neocortical slices[31] demonstrated that proportionally balanced excitation and inhibition enables self-sustaining activity mediated by recurrent excitatory connections, termed "up-states". Cortical up-states occur spontaneously in acute brain slices bathed in solutions that enhance excitability and also can be triggered by synaptic stimulation[31,32]. While these "up-states" can form representations of a single stimulus

(whether a stimulus was presented or not), these network states are not synapse specific[31]. By contrast, PP-evoked hilar synaptic barrages are highly synapse specific and are capable of representing at least four distinct patterns. Cortical networks also exhibit spontaneous neuronal avalanches that persist for 10s of ms[33], a much faster time scale than that of the persistent activity reported here.

In addition to representing specific stimulus locations, we find that hilar synaptic barrages accurately represented temporal sequences of stimuli. Rather than simply trigger stereotyped, stimulus-specific activity patterns, stimulus sequences typically triggered new activity patterns that were distinct from those evoked by the final stimulus in the train (*ABCD* was different from *D* presented alone; Supplemental Fig. 8). This context dependence of stimulus representation, where the response to a specific stimulus was dependent on prior stimuli, also was apparent when synaptic inputs during sequence trains were analyzed (Fig. 6e). Surprisingly, classification accuracy for decoding temporal sequences was robust to a perturbation in sequence interval (Fig. 7d), suggesting that context dependence arises primarily from the relative order of the stimuli. Semilunar granule cells often receive inhibitory postsynaptic responses following hilar and molecular layer stimulation[25] that could provide a cellular substrate for context dependence.

While sequence memory often involves the hippocampal formation[1] and has been demonstrated in computational models of cortical networks[34–37], reliable short-term storage of temporal information has only been infrequently demonstrated at the cellular level. While Branco et al.[38] recently used focal glutamate uncaging at multiple sites along one dendrite to generate sequence-dependent intracellular responses, this mechanism presumably operates primarily through rapid cell-autonomous mechanisms. By contrast, the dentate gyrus circuits activated in the present study reliably encoded temporal sequences with substantially longer time intervals and could be decoded accurately only by comparing activity across multiple simultaneously-recorded hilar cells. Multiple groups have identified "state-dependent" network responses *in vitro*[39] and *in vivo*[40] that reflect the history of previously presented stimuli. While the contextual responses we report in the dentate gyrus *in vitro* likely reflect state-dependent processes, our results differ from previous reports in several respects. We find that hilar networks represent information over longer time periods (many seconds) compared with previous state-dependent studies[39,40]. Hilar networks can encode the order of temporal sequences, not only immediately following the sequence, but also for several seconds afterward. Finally, our results demonstrate rapid encoding of information while previous *in vitro* work required many repeated presentations of stimuli[39], implying a gradual entrainment or learning process.

Relationship to delay-period activity recorded during working memory tasks

Much of our understanding of the cellular basis of short-term information storage is based on classic extracellular recording studies that demonstrated persistent spiking of neocortical[3,6,8,27] and hippocampal[4,7] units during the delay period of short-term memory tasks. These studies showed that the particular units recruited during the delay period depended on the stimulus type (e.g., spatial location) and that delay-period activity was typically absent or reduced in trials when the preferred stimulus was presented and the

subject made an incorrect behavioral response[3,27]. Extracellular recording studies have demonstrated elevated firing frequencies for as long as 20 s during working memory tasks[5,41], arguing that cortical networks must contain mechanisms that support persistent activity over this time scale. However, neurons with a diversity of persistent firing durations typically contribute to delay-period activity during working memory tasks and only a fraction are typically active during the entire delay phase. The subset of delay-period neurons with prolonged persistent activity may play a critical role as "summators" that integrate activity from neurons that are active over different time scales[6,8]. While it is difficult to determine the kinetics of the mechanisms underlying persistent activity during working memory tasks since the learned motor output typically extinguishes persistent firing[3], our experiments demonstrate that the circuitry contained in transverse hippocampal slices, including SGCs with intrinsic persistence, are sufficient to represent information over these long behavioral time scales. Multiple studies[8,42] have demonstrated that compact representations based on population decoding approaches can accurately predict behavioral responses in working memory tasks. Similarly, preserving the heterogeneity in hilar cell responses while ignoring differences in the overall amplitude of responses (i.e., normalization) maintained accurate decoding in our experiments. By contrast, average rate-based coding schemes that ignored the differential contribution of each neuron to the population response failed to classify accurately either location or sequence stimuli.

One likely function of dentate gyrus neurons *in vivo* hypothesized by Marr[43] and subsequent researchers [44] is to transform highly overlapping entorhinal input patterns into more distinct output patterns. While this potential functional role has only recently begun to be tested experimentally[45,46], our demonstration that multiple, reproducible population patterns can be generated in dentate gyrus neurons is consistent with the hypothesis that the neural networks in this brain region can stably represent multiple population patterns. Semilunar granule cells may play an important role during pattern decorrelation by generating a "latch" function that enables hilar neurons to maintain their activity following the transient presentation of a particular entorhinal input pattern. Future *in vivo* studies will be required to follow the downstream consequences of hilar persistent activity since most of the axonal projections of mossy cells extend to distant ipsilateral and contralateral granule cells[29,47], which are not present in transverse hippocampal slices.

The largely feedforward local circuits that appear to support short-term storage of information in the dentate gyrus suggest a fundamentally different mechanism than the recurrent excitatory networks commonly employed in artificial neural network models of working memory[10–13]. Despite extensive efforts to identify biological persistent activity modes mediated by recurrent excitatory synaptic connections[48], very little experimental evidence supports the classic hypothesis that reverberant network activity functions to encode and maintain information proposed by Hebb[9]. Our finding that sequential stimulation did not reset hilar persistent activity to a new state corresponding to the most recent stimulus is also inconsistent with the predictions from theoretical studies employing attractor-based networks with recurrent connectivity[49]. At the other extreme, multiple groups have demonstrated neuron cell types that can fire persistently following transient stimuli through cell-autonomous intrinsic mechanisms[16,17] and several theoretical studies

have demonstrated that combining intrinsic persistence with recurrent excitatory connections relaxes the requirements for precise tuning of synaptic weights[11,14,18,19]. The alternative intrinsic/feedforward mechanism we hypothesize enables hilar neurons to represent stimulus and sequence identity is related to a recent theoretical study[37] arguing that purely feedforward circuits can generate prolonged network activity when the effective network time constant is extended by creating multiple serial processing stages. Presumably, the number of stages required to generate delay-period activity would be reduced if some stages of the feedforward network employed neurons with intrinsic persistence, such as SGCs.

The dentate gyrus is unusual in the high frequency of spontaneous synaptic activity recorded in hilar neurons and because of semilunar granule cells, a subtype of excitatory projection with multistability under standard physiological conditions. Populations of hilar neurons presumably can encode stimulus and sequence identity in our experiments because at least some divergent SGC-to-hilar neuron synaptic connections are preserved in conventional horizontal brain slices. Revealing persistent activity modes in the dentate gyrus was facilitated by the anatomical separation of multistable excitatory neurons (SGCs) and downstream hilar neurons. However, other examples of bistability and multistability of excitatory projection neurons in more hetereogenous brain regions have been reported following bath application of modulatory neurotransmitters, raising the possibility that the hybrid intrinsic/feedforward mechanism we propose in the dentate gyrus may be generalizable. For example, a subclass of neurons in entorhinal cortex are capable of persistent firing following transient stimulation in the presence of muscarinic receptor agonists[16]. To date, no group has reported whether activation of different synaptic inputs to entorhinal cortex leads to mnemonic encoding. Transient inputs also can trigger cell-autonomous persistent firing in neocortical neurons when intrinsic excitability is enhanced following cholinergic receptor activation[50], providing a potential connection between intrinsic/feedforward persistent mechanisms we propose in the dentate gyrus and classic delay-period activity recorded in prefrontal cortical neurons *in vivo*.

METHODS

Methods and associated references are available in the online version of the paper.

ONLINE METHODS

Animals

Horizontal slices (300 μm thick) of the ventral hippocampus were prepared from P14-25 Sprague-Dawley rats anesthetized with ketamine, as described previously [20,30]. Slices were incubated at 30 °C for 30 min and then maintained at room temperature until needed. All experiments were carried out under guidelines approved by the Case Western Reserve University Animal Care and Use Committee.

Electrophysiology

All intracellular recordings were performed in a submerged recording chamber maintained at 30°C and perfused with an extracellular solution containing (in mM): 124 NaCl, 3 KCl, 1.23 NaH2PO4, 1.2 MgSO4, 26 NaHCO3, 10 dextrose, 2.5 CaCl$_2$, equilibrated with 95%

O_2/5% CO_2 (pH 7.3). Whole-cell patch clamp recordings were made using AxoPatch 1D amplifiers (Molecular Devices) and borosilicate glass pipettes (3-10 MΩ). Recording electrodes contained (in mM): 140 K methylsulfate, 4 NaCl, 10 HEPES, 0.2 EGTA, 4 MgATP, 0.3 Na3GTP, 10 phosphocreatine, adjusted to pH 7.3 and ~ 290 mOsm. Individual neurons were visualized under IR-DIC video microscopy (Zeiss Axioskop FS1) prior to patch-clamp recording. We typically restricted our experiments to a set of two or three nearby hilar cells with inter-soma distances less than 100 μm. Intracellular recordings were low-pass filtered at 2 kHz (FLA-01, Cygnus Technology) and acquired at 5 kHz using a simultaneously-sampling 16-bit data acquisition system (ITC-18, Instrutech) operated by custom software written in VB.NET (Microsoft) and Matlab (Mathworks). Intracellular voltages were not corrected for the liquid junction potential. A matrix microelectrode consisting of 4 sharpened tungsten monopolar electrodes (115 μm spacing; FHC) was used for extracellular stimulation. Stimulus intensity was controlled by a custom-built constant-voltage stimulus isolation unit. Hilar barrages were evoked most reliably by paired stimuli (500 ms inter-stimulus intervals), as described previously [20]. All population responses reported in this study reflect paired stimuli at this interval; responses to sequential stimuli (e.g., *ABCD*) reflect paired shocks at each matrix electrode contact at the indicated interval (paired shocks every 4-120 s). Hilar recordings and population responses were typically stable over 10-15 paired stimuli or temporal sequences of different stimuli (3.5 min delay between different stimuli in both experiment types, except for 120 s sequential stimuli experiments). We collected the data set of experiments using different stimulus locations in one continuous series after an initial set of pilot studies to optimize stimulus and recording conditions. Only experiments in which hilar cell recordings degraded or in which we obtained fewer than 3 responses from each stimulus type were excluded from the analysis.

Data analysis and statistics

Hilar cells were identified by their intrinsic properties (mean spike time, spike clustering, and spike AHP) following 4 s-duration depolarizing and hyperpolarizing current steps, as described previously [30]. Most recordings in this study were from presumptive hilar mossy cells. Spontaneous EPSPs were identified automatically using a custom detection algorithm [30]. Except where noted, all data are presented as mean ± SEM. Statistical significance was determined using Student's *t*-test, unless otherwise specified.

Analysis of hilar population responses

EPSPs were typically detected in a 4-s window that began 0.5 s after the last shock of each paired stimulus. The mean EPSP frequency within this window in each recorded hilar cell was used to analyze population responses. We approached the question of whether population responses evoked by different stimulus electrodes were distinct using three complementary methods. First, we assessed the separability of population responses by calculating the overlap coefficient (OVL [51,52]; Supplemental Fig. 3). In this method, we computed the distribution of Euclidean distances from individual population responses (the mean EPSP frequencies in the same 4 s analysis window applied to each simultaneously-recorded hilar cell) with the centroid calculated from all responses evoked by the stimulus electrode in the same experiment ("Cis" distances). The distribution of these Cis distances was then compared with the distribution of "Trans" distances calculated from dissimilar data

point/centroid pairs (e.g., A points to the centroid of all B points). The overlap coefficient OVL was computed from Gaussian fits of Cis and Trans distributions. The statistical significance of the OVL coefficient was determined by bootstrap methods (20,000 randomizations of Cis/Trans labels on each actual distance). All location experiments analyzed in this study yielded statistically distinct Cis/Trans distributions (all OVL calculated reflected P<0.05; Fig. 2e).

Second, we used linear discriminant analysis (LDA [53–55]) to determine the number of statistically separable population responses in each experiment. Complete classification of population responses to all 4 stimulus locations (*A-D*) required 6 statistically significant pairwise LDA tests (*A/B*, *B/C*, etc), each with P<0.0083 reflecting a Bonferroni correction for multiple comparisons. Plots of the number of discrimination planes in different conditions (Fig. 2d, Fig. 8d-e, Supplemental Fig. 2) reflect the number of pairwise LDA tests with P < 0.05. We estimated the number of planes expected by chance by randomly re-assigning EPSP frequencies in each hilar cell to different stimulus identities. We recalculated the number of statistically significant LDA planes following 30 iterations to generate an estimate of the number of planes expected by chance. A statistically significant OVL coefficient combined with 6/6 possible LDA tests (with P < 0.0083) represents a conservative test for response separability, a criterion that was met in 50% of the experiments we analyzed. If one experiment failed to generate 4 separable responses, it was re-analyzed to determine if three (3 appropriate planes with P<0.016) or two (one plane with P<0.05) responses could be isolated. We calculated the time course of response separability using a sliding 4-s window and repeated the LDA at 1 s intervals. Times indicated reflect the beginning of each 4-s time window. We also used LDA based on the mean EPSP frequency in 4-s windows that began 0.5 s after the last stimulus in each sequence (e.g., 0.5 s after the *D* in *ABCD* and after the *A* in *DCBA*) to determine if population responses to different temporal sequences were significantly different. We employed the same time windows when analyzing sequences with both 4- and 5-s intervals.

Finally, we assessed the accuracy of hilar population responses in predicting stimulus identity, assayed by nearest stimulus centroid. Classification accuracy was calculated for the entire data set from the ratio of trials classified correctly to the total number of trials tested. Sequence identity was predicted from the sign of the response distance to the LDA plane.

Character intensity plots (Fig. 5 and Supplemental Fig. 5) reflect the relative Euclidean distances between each population response and the four stimulus centroids, recomputed at 1 s intervals. Each location reflects the superposition of four characters (A,B,C,D) whose intensities are scaled to reflect their relative distance to stimulus centroids. The scaling function was normalized by the sum of the scaled distances to all four centroids:

$$Intensity = \frac{e^{-\sqrt{d_x}}}{e^{-\sqrt{d_1}} + e^{-\sqrt{d_2}} + e^{-\sqrt{d_3}} + e^{-\sqrt{d_4}}}$$

where *d* represents the Euclidean distance between a single response and a response centroid and *x* is the stimulus identity being tested. This transformation resulted in one very dark

(high contrast) character superimposed on three light (low contrast) characters if a response was very close to a stimulus centroid. We then iterated through all four possible centroids at each time step:

$$p_{ijk} = \frac{e^{-\sqrt{d_{ijk}}}}{\sum_{i=1}^{4} e^{-\sqrt{d_{ijk}}}}$$

$$d_{ijk} = \left| \overrightarrow{F}_{ijk} - \overrightarrow{F}^{c}_{ij} \right|$$

where p is character intensity, i represents stimulus identity, j represents the time bin, k represents the trial, and F^C represents the centroid vector for one stimulus identity at one time bin. The relative distance between forward and reverse responses in Fig. 7c was calculated as the signed length of the projection of the population responses onto the difference vector:

$$D_i = \frac{\overrightarrow{F}_i \cdot \overrightarrow{\delta}_{FR}}{\left| \overrightarrow{\delta}_{FR} \right|}$$

where δ represents the difference vector of the mean population responses for forward and reverse sequences and F is the population response vector. Data analysis was performed in Matlab (Mathworks) and Origin (OriginLab).

Supplementary Material

Refer to Web version on PubMed Central for supplementary material.

ACKNOWLEDGEMENTS

References

1. Fortin NJ, Agster KL, Eichenbaum HB. Critical role of the hippocampus in memory for sequences of events. Nat. Neurosci. 2002; 5:458–462. [PubMed: 11976705]

2. Averbeck BB, Lee D. Prefrontal neural correlates of memory for sequences. J. Neurosci. 2007; 27:2204–2211. [PubMed: 17329417]

3. Funahashi S, Bruce CJ, Goldman-Rakic PS. Mnemonic coding of visual space in the monkey's dorsolateral prefrontal cortex. J. Neurophysiol. 1989; 61:331–349. [PubMed: 2918358]

4. Colombo M, Gross CG. Responses of inferior temporal cortex and hippocampal neurons during delayed matching to sample in monkeys (Macaca fascicularis). Behav. Neurosci. 1994; 108:443–455. [PubMed: 7917038]

5. Fuster JM, Jervey JP. Inferotemporal neurons distinguish and retain behaviorally relevant features of visual stimuli. Science. 1981; 212:952–955. [PubMed: 7233192]

6. Batuev AS, Kursina NP, Shutov AP. Unit activity of the medial wall of the frontal cortex during delayed performance in rats. Behav. Brain Res. 1990; 41:95–102. [PubMed: 2288669]

7. Hampson RE, Heyser CJ, Deadwyler SA. Hippocampal cell firing correlates of delayed-match-to-sample performance in the rat. Behav. Neurosci. 1993; 107:715–739. [PubMed: 8280383]

8. Baeg EH, et al. Dynamics of population code for working memory in the prefrontal cortex. Neuron. 2003; 40:177–188. [PubMed: 14527442]

9. Hebb, DO. The organization of behavior: A neuropsychological theory. John Wiley & Sons; New York: 1949.

10. Seung HS. How the brain keeps the eyes still. Proc. Natl. Acad. Sci. U.S.A. 1996; 93:13339–13344. [PubMed: 8917592]

11. Camperi M, Wang XJ. A model of visuospatial working memory in prefrontal cortex: recurrent network and cellular bistability. J Comput Neurosci. 1998; 5:383–405. [PubMed: 9877021]

12. Compte A, Brunel N, Goldman-Rakic PS, Wang XJ. Synaptic mechanisms and network dynamics underlying spatial working memory in a cortical network model. Cereb. Cortex. 2000; 10:910–923. [PubMed: 10982751]

13. Miller P, Brody CD, Romo R, Wang X-J. A recurrent network model of somatosensory parametric working memory in the prefrontal cortex. Cereb. Cortex. 2003; 13:1208–1218. [PubMed: 14576212]

14. Seung HS, Lee DD, Reis BY, Tank DW. Stability of the memory of eye position in a recurrent network of conductance-based model neurons. Neuron. 2000; 26:259–271. [PubMed: 10798409]

15. Mensh BD, Aksay E, Lee DD, Seung HS, Tank DW. Spontaneous eye movements in goldfish: oculomotor integrator performance, plasticity, and dependence on visual feedback. Vision Res. 2004; 44:711–726. [PubMed: 14751555]

16. Egorov AV, Hamam BN, Fransén E, Hasselmo ME, Alonso AA. Graded persistent activity in entorhinal cortex neurons. Nature. 2002; 420:173–178. [PubMed: 12432392]

17. Pressler RT, Strowbridge BW. Blanes cells mediate persistent feedforward inhibition onto granule cells in the olfactory bulb. Neuron. 2006; 49:889–904. [PubMed: 16543136]

18. Koulakov AA, Raghavachari S, Kepecs A, Lisman JE. Model for a robust neural integrator. Nat. Neurosci. 2002; 5:775–782. [PubMed: 12134153]

19. Goldman MS, Levine JH, Major G, Tank DW, Seung HS. Robust persistent neural activity in a model integrator with multiple hysteretic dendrites per neuron. Cereb. Cortex. 2003; 13:1185–1195. [PubMed: 14576210]

20. Larimer P, Strowbridge BW. Representing information in cell assemblies: persistent activity mediated by semilunar granule cells. Nat. Neurosci. 2010; 13:213–222. [PubMed: 20037579]

21. MacVicar BA, Dudek FE. Local synaptic circuits in rat hippocampus: interactions between pyramidal cells. Brain Res. 1980; 184:220–223. [PubMed: 6244052]

22. Miles R, Wong RK. Excitatory synaptic interactions between CA3 neurones in the guinea-pig hippocampus. J. Physiol. (Lond). 1986; 373:397–418. [PubMed: 3018233]

23. Song S, Sjöström PJ, Reigl M, Nelson S, Chklovskii DB. Highly nonrandom features of synaptic connectivity in local cortical circuits. PLoS Biol. 2005; 3:e68. [PubMed: 15737062]

24. Acsády L, Kamondi A, Sík A, Freund T, Buzsáki G. GABAergic cells are the major postsynaptic targets of mossy fibers in the rat hippocampus. J. Neurosci. 1998; 18:3386–3403. [PubMed: 9547246]

25. Williams PA, Larimer P, Gao Y, Strowbridge BW. Semilunar granule cells: glutamatergic neurons in the rat dentate gyrus with axon collaterals in the inner molecular layer. J. Neurosci. 2007; 27:13756–13761. [PubMed: 18077687]

26. Gupta A, Elgammal FS, Proddutur A, Shah S, Santhakumar V. Decrease in tonic inhibition contributes to increase in dentate semilunar granule cell excitability after brain injury. J. Neurosci. 2012; 32:2523–2537. [PubMed: 22396425]

27. Funahashi S, Chafee MV, Goldman-Rakic PS. Prefrontal neuronal activity in rhesus monkeys performing a delayed anti-saccade task. Nature. 1993; 365:753–756. [PubMed: 8413653]

28. Crowe DA, Averbeck BB, Chafee MV. Rapid sequences of population activity patterns dynamically encode task-critical spatial information in parietal cortex. J. Neurosci. 2010; 30:11640–11653. [PubMed: 20810885]

29. Buckmaster PS, Wenzel HJ, Kunkel DD, Schwartzkroin PA. Axon arbors and synaptic connections of hippocampal mossy cells in the rat in vivo. J. Comp. Neurol. 1996; 366:271–292. [PubMed: 8698887]

30. Larimer P, Strowbridge BW. Nonrandom local circuits in the dentate gyrus. J. Neurosci. 2008; 28:12212–12223. [PubMed: 19020015]

31. Shu Y, Hasenstaub A, McCormick DA. Turning on and off recurrent balanced cortical activity. Nature. 2003; 423:288–293. [PubMed: 12748642]

32. MacLean JN, Watson BO, Aaron GB, Yuste R. Internal dynamics determine the cortical response to thalamic stimulation. Neuron. 2005; 48:811–823. [PubMed: 16337918]

33. Beggs JM, Plenz D. Neuronal avalanches in neocortical circuits. J. Neurosci. 2003; 23:11167–11177. [PubMed: 14657176]

34. Abbott LF, Blum KI. Functional significance of long-term potentiation for sequence learning and prediction. Cereb. Cortex. 1996; 6:406–416. [PubMed: 8670667]

35. Diesmann M, Gewaltig MO, Aertsen A. Stable propagation of synchronous spiking in cortical neural networks. Nature. 1999; 402:529–533. [PubMed: 10591212]

36. Mongillo G, Barak O, Tsodyks M. Synaptic theory of working memory. Science. 2008; 319:1543–1546. [PubMed: 18339943]

37. Goldman MS. Memory without feedback in a neural network. Neuron. 2009; 61:621–634. [PubMed: 19249281]

38. Branco T, Clark BA, Häusser M. Dendritic discrimination of temporal input sequences in cortical neurons. Science. 2010; 329:1671–1675. [PubMed: 20705816]

39. Johnson HA, Goel A, Buonomano DV. Neural dynamics of in vitro cortical networks reflects experienced temporal patterns. Nat. Neurosci. 2010; 13:917–919. [PubMed: 20543842]

40. Nikoli D, Häusler S, Singer W, Maass W. Distributed fading memory for stimulus properties in the primary visual cortex. PLoS Biol. 2009; 7:e1000260. [PubMed: 20027205]

41. Miyashita Y, Chang HS. Neuronal correlate of pictorial short-term memory in the primate temporal cortex. Nature. 1988; 331:68–70. [PubMed: 3340148]

42. Barak O, Tsodyks M, Romo R. Neuronal population coding of parametric working memory. J. Neurosci. 2010; 30:9424–9430. [PubMed: 20631171]

43. Marr D. Simple memory: a theory for archicortex. Philos. Trans. R. Soc. Lond., B, Biol. Sci. 1971; 262:23–81. [PubMed: 4399412]

44. Rolls ET, Treves A. Neural networks in the brain involved in memory and recall. Prog. Brain Res. 1994; 102:335–341. [PubMed: 7800823]

45. Leutgeb JK, Leutgeb S, Moser M-B, Moser EI. Pattern separation in the dentate gyrus and CA3 of the hippocampus. Science. 2007; 315:961–966. [PubMed: 17303747]

46. McHugh TJ, et al. Dentate gyrus NMDA receptors mediate rapid pattern separation in the hippocampal network. Science. 2007; 317:94–99. [PubMed: 17556551]

47. Deadwyler SA, West JR, Cotman CW, Lynch GS. A neurophysiological analysis of commissural projections to dentate gyrus of the rat. J. Neurophysiol. 1975; 38:167–184. [PubMed: 162942]

48. Aksay E, et al. Functional dissection of circuitry in a neural integrator. Nat. Neurosci. 2007; 10:494–504. [PubMed: 17369822]

49. Brunel N, Wang XJ. Effects of neuromodulation in a cortical network model of object working memory dominated by recurrent inhibition. J Comput Neurosci. 2001; 11:63–85. [PubMed: 11524578]

50. Krnjevi K, Phillis JW. Pharmacological properties of acetylcholine-sensitive cells in the cerebral cortex. J. Physiol. (Lond.). 1963; 166:328–350. [PubMed: 16992146]

51. Inman HF, Bradley EL. The overlapping coefficient as a measure of agreement between probability distributions and point estimation of the overlap of two normal densities. Communications in Statistics - Theory and Methods. 1989; 18:3851–3874.

52. Clemons TE, Bradley EL. A nonparametric measure of the overlapping coefficient. Computational Statistics & Data Analysis. 2000; 34:51–61.

53. Fisher RA. The use of multiple measurements in taxonomic problems. Annals Human Genetics. 1936; 7:179–188.

54. Klecka, W. Discriminant Analysis. Sage Publications; Newbury Park, CA: 1980.

55. MacLeod K, Bäcker A, Laurent G. Who reads temporal information contained across synchronized and oscillatory spike trains? Nature. 1998; 395:693–698. [PubMed: 9790189]
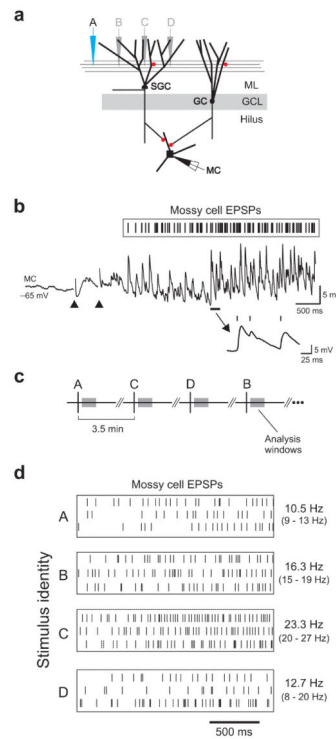
Figure 1. Persistent synaptic activity evoked by multiple PP stimuli

a, Experimental configuration. A four-position stimulating electrode was used to activate different PP segments while recording synaptic input in hilar neurons. **b**, Example of a hilar mossy cell synaptic barrage evoked by PP stimulation (arrow heads). The timing of the onsets of individual EPSPs is indicated by vertical lines. Enlargement of region indicated with horizontal bar shown in *inset*. **c**, Experimental protocol and EPSP analysis windows. **d**, Responses to three repetitions of each of the four stimulus positions (A-D) in one hilar mossy cell. Vertical lines indicate EPSP onset times. Mean EPSP frequency and range for each stimulus type indicated on *right*. Diagram of experiment protocol shown at *top*.
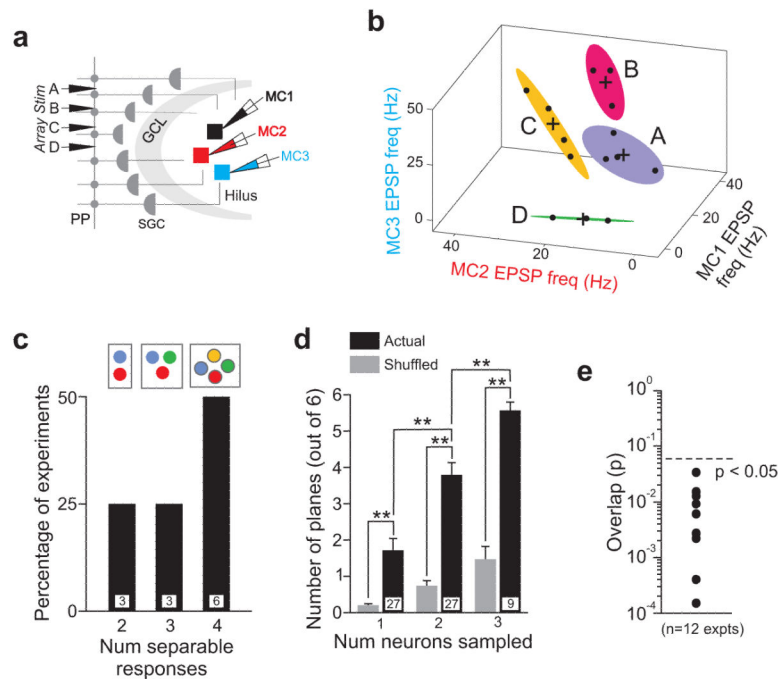
Figure 2. Short-term hilar representations of multiple PP stimuli

a, Triple hilar cell recording configuration. **b,** Stimulation at different sites evokes distinct synaptic barrages in hilar networks. Summary plot of mean EPSP frequency during initial 4 s of barrages following PP stimulation in one experiment. Black dots represent 14 consecutive single trials, crosses represent centroids of each trial type (stimulus A, B, etc). Shaded zones represent bounding ellipsoids used to illustrate variance associated with repeated responses to the same stimulus (60% confidence intervals). **c,** Histogram of experiments with 2, 3 and 4 statistically separable responses over 12 experiments. **d,** Plot of the number of statistically significant ($P < 0.05$) planes obtained by LDA in the 9 triple recording experiments (black bars) and following shuffling stimulus identity (grey bars). Results are presented from LDA computed on data from all three simultaneous recordings (right set of bars; $n = 9$) and when only one ($n=27$) and two neurons ($n=27$) are considered. ** $P < 0.01$. **e,** Plot of probabilities associated with the overlap coefficient (OVL) for the same 12 experiments. Dashed line indicates statistically significant OVL range ($P < 0.05$). See text and Supplemental Fig. 3 for details.
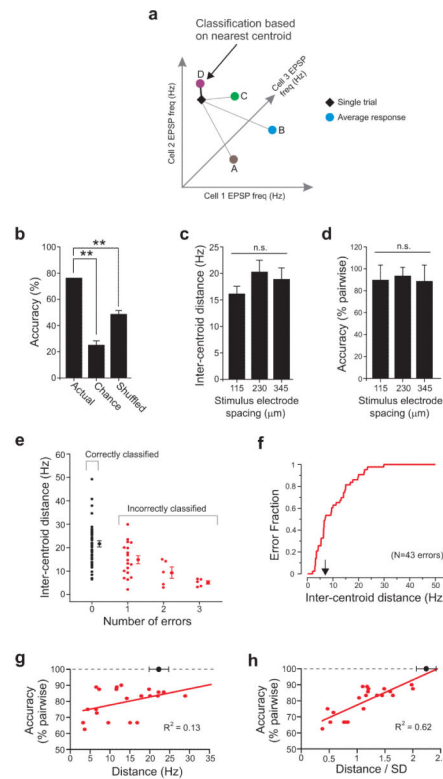
Figure 3. Prediction of stimulus identity from hilar population responses
a, Analysis method based on computing Euclidean distance from each response (black diamond) to the four centroids (filled circles) that represent average responses to each type of stimuli. **b**, Plot of mean accuracy in predicting stimulus identity (A-D) based on the nearest average response centroid, compared with accuracies expected by chance. ** $P <$ 0.0001. **c**, Plot of the average Euclidean distance between pairs of response centroids evoked by adjacent (115 μm separation) and non-adjacent (230 and 345 μm separation) stimulating electrode contacts. **d**, Plot of accuracy of predicting stimulus identity based on nearest centroid versus stimulus electrode separation. Pairs of stimuli evoked on adjacent electrode contacts were classified as accurately as stimuli evoked by non-adjacent pairs. Accuracy expected by chance was 50% in this pairwise analysis. **e**, Distribution of inter-centroid distances between pairs of responses that were correctly (black symbols) and incorrectly (red symbols) classified. Number of errors associated with each inter-centroid distance plotted on X axis. Mean ± SEM of distance for correctly (black circle) and incorrectly (red circle) classified response pairs plotted next to each distribution. **f**, Cumulative distribution of distances associated with classification errors. Half of the classification errors results from comparisons between response centroids separated by less than 7 Hz (arrow on X axis). **g**, Plots of accuracy classifying response pairs with occasional errors versus inter-centroid distance. **h**, Plot of accuracy classifying response pairs with occasional errors versus distance/S.D. ratio. Solid lines represent linear regression fits in both *g* and *h*. Black symbols represent the mean Euclidean distance (in *g*) and distance/S.D. ratio (in *h*) associated with response pairs that were always classified correctly.
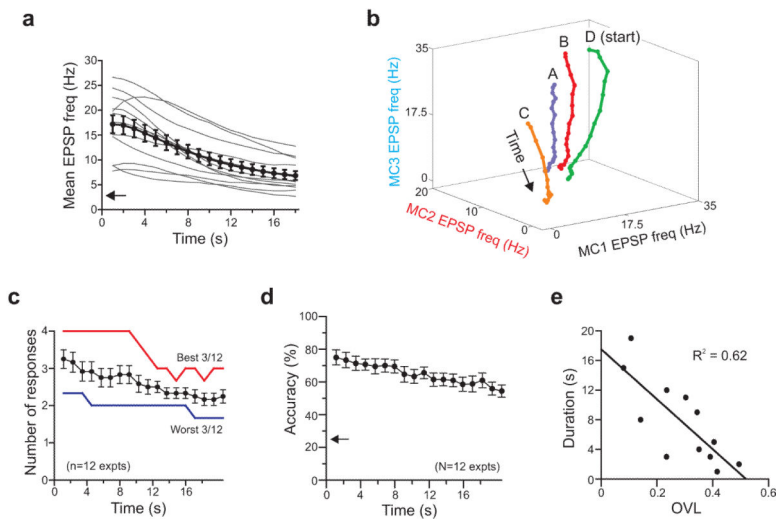
Figure 4. Time course of hilar population responses

a, Plot of decay of average EPSP frequency during synaptic barrages in 12 experiments (thin lines represent each experiment; symbols represent overall mean ± SEM). Arrow on Y axis indicates average baseline EPSP frequency. **b**, Plot of centroid position as response evolves over time in one experiment (18 sliding 4-s windows). Each point reflects mean EPSP frequency in three hilar cells over a 4-s window. **c**, Plot of the number of statistically separable responses (out of 4 possible) versus time. Symbols represent mean ± SEM (*n*=12 experiments). Red and blue lines represent best and worst three experiments, respectively (see text). **d**, Plot of classification accuracy over time using the entire data set. Arrow along Y axis indicates accuracy expected by chance. **e**, The initial response overlap coefficient (OVL) is negatively correlated ($R^2 = 0.62$; *P* < 0.005; *F* = 15.4; *n* = 12 experiments) to the duration responses evoked by different stimuli are significantly distinguishable.
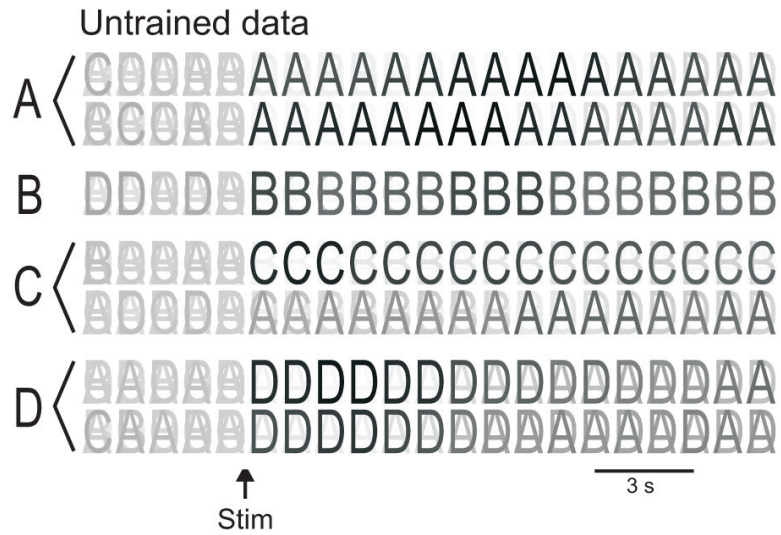
Figure 5. Visual display of cross-validated data

Graphical representation of response classification using only untrained data. Half of the episodes were used to compute response centroids; character plots were generated from the remaining 50% of episodes. All the episodes from the same experiment plotted using the same display algorithm in Supplemental Figure 5.
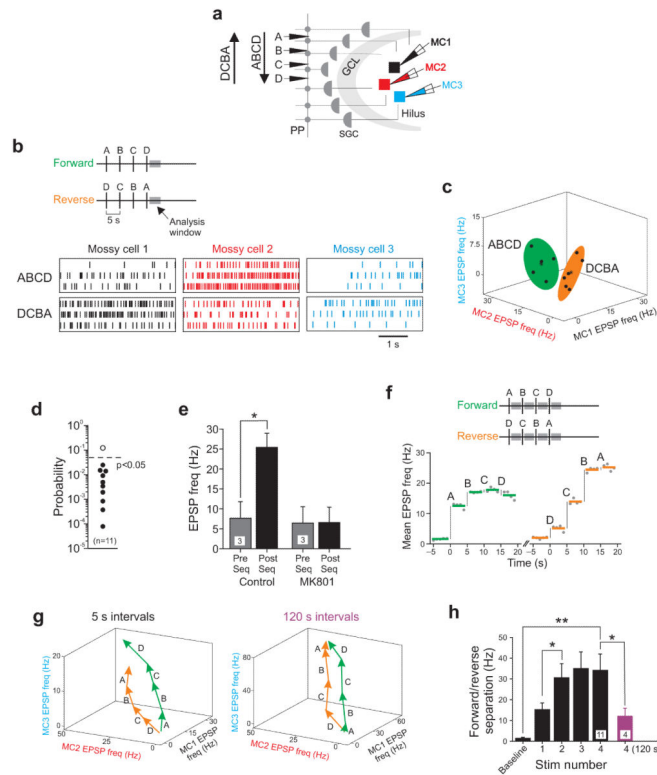
Figure 6. Short-term representations of temporal sequences in hilar neurons
a, Experimental configuration. **b**, Responses to three trials of forward (ABCD) and reverse
(DCBA) temporal stimuli sequences recorded intracellularly from three hilar cells. Vertical
lines represent EPSP onset times. **c**, Plot of individual responses to forward and reverse
sequential stimulation (black circles) in EPSP frequency space (5 forward and 6 reverse,
acquired in pseudo-random order; 4 s analysis window after final stimulus in each
sequence). All points contained within bounding ellipsoids (60% confidence interval, as in
Fig. 2b) centered on response centroids (black asterisks). **d**, Plot of probabilities that forward
and reverse points are significantly different by LDA. Forward and reverse sequences were
significantly different (P <0.05) in 10/11 experiments (filled symbols) and not different in
one experiment (open symbol). **e**, Plot of the effect of MK801 (10 μM) on the mean EPSP
frequencies in three sequential stimulation experiments. Population responses to forward and
reverse sequential stimulation were separable using LDA in control conditions in each
experiment (before MK801; all $P < 0.05$). Sequential stimulation triggered a mean increase
of 17.8 Hz in control conditions in these three experiments, not statistically different than
the 16.1 Hz increase observed in the larger set of 12 sequential stimulation experiments.
Sequential stimulation failed to trigger an increase in EPSP frequency in MK801 ($P > 0.05$).
* $P < 0.05$. **f**, Plot of mean EPSP frequency across a triple recording for all forward and
reverse sequences tested in one experiment. Horizontal bars indicate mean EPSP frequency
for baseline period and for 4-s windows following each stimuli within the sequence. **g**,
Vector representation of average population response to forward and reverse sequences.
Responses to each stimuli were combined head-to-tail and failed to converge for fast (5 s
intervals, left) sequences but converged for slow (120 s intervals, right) sequences in a
different experiment. **h**, Plot of average separation in head-to-tail vector representations of

forward and reverse sequences (similar to *g*) over 11 experiments. Black bars represent results from 5 s sequences; purple bar represents forward/reverse separation at the end of 120 s sequences. * *P* < 0.05; ** *P* < 0.0005. Mean ± SEM.
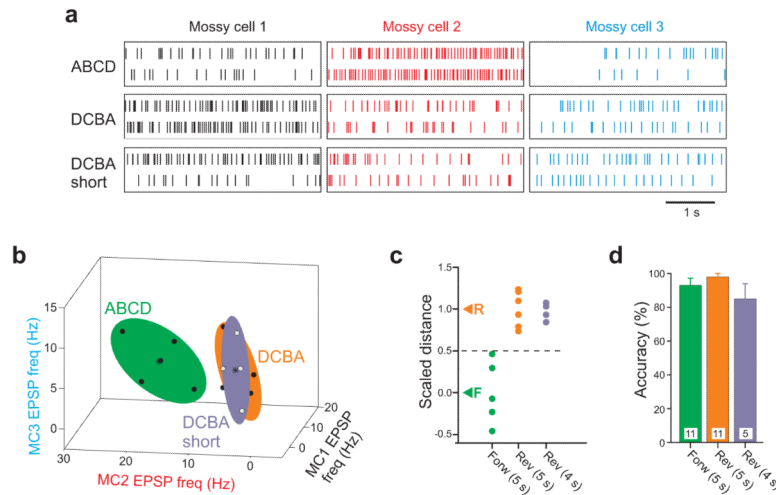
Figure 7. Sequence representations are robust to perturbation of stimulus interval

a, Example of EPSP responses to forward and reverse sequential stimuli at 5 s intervals (*ABCD*, *DCBA*) and reverse stimuli at 4 s intervals (*DCBA short*) recorded in three hilar mossy cells. **b**, Plot of forward (black symbols within green ellipsoid), reverse (black symbols within orange ellipsoid) and reverse short (white points within purple ellipsoid) responses in EPSP frequency space in one experiment. Response centroids indicated by asterisks (reverse and reverse short centroid symbols overlap); colored ellipsoids represent 60% confidence intervals. **c**, Plot of scaled distance between forward (black symbols) and reverse (orange) 5 s interval sequence responses in one experiment. Responses to 4-s reverse responses (purple symbols) overlapped the 5 s reverse responses. Over 5 experiments, the mean scaled distance of the 4 s reverse points was 0.72; significantly different from 5 s forward responses ($P < 0.005$) and not significantly different from 5 s reverse responses ($P > 0.05$). **d**, Plot of classification accuracy for experiments with forward (green bar; $n = 11$), reverse (orange bar; $n = 11$) 5 s interval sequences, and reverse sequences with 4 s intervals (purple bar; $n = 5$). Mean accuracies not statistically different from each other, $P > 0.05$. Mean ± SEM.
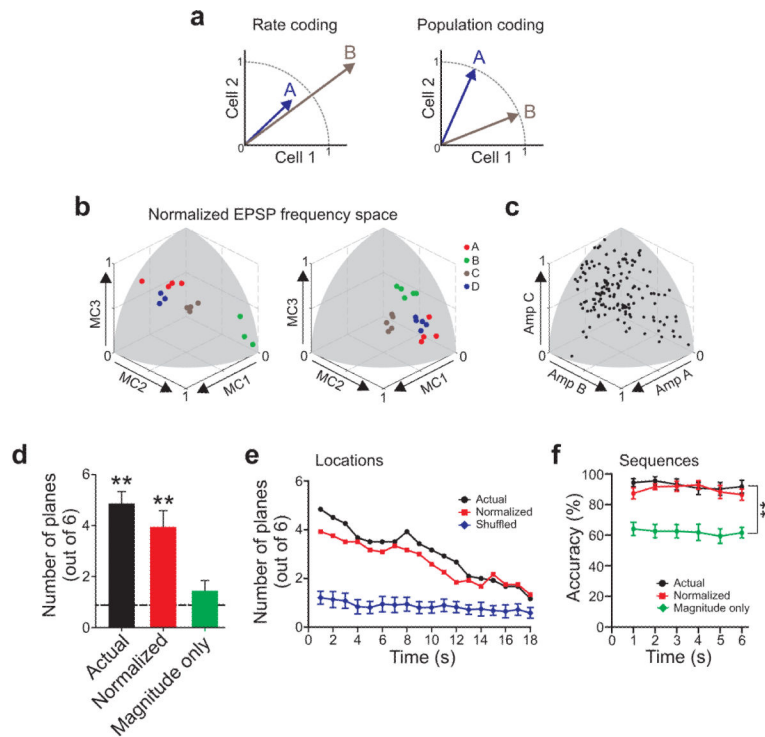
Figure 8. Population representations of stimulus and sequence identity in the dentate gyrus
a, Diagram illustrating rate and population coding strategies. **b**, Plots of responses to 4 different stimulus positions in normalized EPSP frequency space from two experiments. **c**, Plot of all responses from 11 experiments in normalized EPSP space. Gray regions represent surface of sphere with unit radius. **d**, Plot of number of statistically significant LDA separation planes ($P < 0.05$) from all experiments with 4 different stimulus locations (*Actual*, $n = 12$), the number of planes in the same data set after normalizing vector magnitudes (*Normalized*), and after eliminating vector direction information (*Magnitude only*). Dashed line indicates mean number of significant LDA planes after shuffling stimulus identities in all 12 experiments. Mean ± SEM. ** Significantly different from shuffled stimulus identities; $P < 0.0001$. Both Actual and Normalized are significantly different from *Magnitude only* ($P < 0.01$); *Actual* and *Normalized* are not significantly different ($P > 0.05$). **e**, Plot of number of statistically significant LDA separation planes ($P < 0.05$; out of 6 possible) over time. Purple symbols indicate mean ± SD number of significant planes after shuffling the stimulus identities. Both actual (black symbols) and normalized responses (red symbols) remained significantly greater than shuffled throughout the time period examined ($P < 0.05$). **f**, Plot of accuracy of predicting sequence identity over time in control conditions (*Actual*, black symbols), following response normalization (red symbols) and using only vector magnitude information (green symbols). Both control (*Actual)* and *Normalized* conditions are significantly different from the *Magnitude only* condition at all time points. ** $P < 0.002$.